PNAS RESEARCH ARTICLE | ENGINEERING

Soft, strong, tough, and durable protein-based fiber hydrogels

Mingkun Wang[a,1], Shuofei Sun[a], Gening Dong[a], Feifei Long[a], and Jonathan T. Butcher[a,1]

Edited by Christopher S. Chen, Boston University, Boston, MA; received July 28, 2022; accepted January 4, 2023 by Editorial Board Member John A. Rogers

Load-bearing soft tissues normally show J-shaped stress–strain behaviors with high compliance at low strains yet high strength at high strains. They have high water content but are still tough and durable. By contrast, naturally derived hydrogels are weak and brittle. Although hydrogels prepared from synthetic polymers can be strong and tough, they do not have the desired bioactivity for emerging biomedical applications. Here, we present a thermomechanical approach to replicate the combinational properties of soft tissues in protein-based photocrosslinkable hydrogels. As a demonstration, we create a gelatin methacryloyl fiber hydrogel with soft tissue-like mechanical properties, such as low Young's modulus (0.1 to 0.3 MPa), high strength (1.1 ± 0.2 MPa), high toughness (9,100 ± 2,200 J/m^3), and high fatigue resistance (2,300 ± 500 J/m^2). This hydrogel also resembles the biochemical and architectural properties of native extracellular matrix, which enables a fast formation of 3D interconnected cell meshwork inside hydrogels. The fiber architecture also regulates cellular mechanoresponse and supports cell remodeling inside hydrogels. The integration of tissue-like mechanical properties and bioactivity is highly desirable for the next-generation biomaterials and could advance emerging fields such as tissue engineering and regenerative medicine.

gelatin methacryloyl | antifatigue hydrogels | microfibers | soft-tissue engineering | mechanosensing

Significance

Emerging biomedical applications, such as tissue engineering and artificial tissues, require implant materials to be both biologically and mechanically compatible with living tissues. However, the combination of these two properties has not been achieved in current material systems. Naturally derived materials carry the essential biological features of tissues but tend to be weak and brittle. Whereas synthetic polymers can replicate the mechanical properties of tissues but often lack the ability to support and direct live cells. Here, we present a strategy to overcome this dilemma. We mimic the hierarchical structure of tissues using protein-based hydrogels such as gelatin. This structure leads to the combination of soft tissue-like mechanical properties, uniform 3D cellularization, and great bioactivity.

Load-bearing soft tissues often demonstrate J-shaped stress–strain behaviors under stretch, and they are soft at small strains but stiffen exponentially with increasing strains (1–3). Despite their high water content of 70 to 80 wt%, tissues maintain their mechanical properties even when used for millions of cycles per year (4, 5).

Replication of all these properties is extremely challenging. Hydrogels with strong and dense crosslinks are strong but rigid (6) and their Young's modulus is usually linear and high even at small strains. Strain-stiffening hydrogels (7), and bottle brush polymer networks (8), can mimic the J-shaped nonlinear elasticity, but their toughness is usually low. Double-network hydrogels exhibit greater toughness because they can dissipate energy via weak physical crosslinks such as hydrogen bonds (9), and electrostatic (10), and hydrophobic interactions (11). However, those mechanisms do not improve their fatigue resistance (12). Hydrogels with strong physical crosslinks such as nanocrystalline domains are fatigue resistant (13), but the strong physical crosslinks again often increase the Young's modulus and decrease the stretchability of hydrogels.

Unlike those homogeneous hydrogels, biological tissues consist of fiber meshwork with diameters typically of the order of micrometers. Their combination of nonlinear Young's modulus, high strength, large toughness, and superior fatigue resistance originates from the hierarchical architectures of microfibers (14, 15). Those fibers reorientate under stretch and create the nonlinear elasticity. They can stiffen and then fracture simultaneously to endow a high tensile strength (16). The fracture of fibers requires a much higher energy per unit area than that for fracturing a single polymer chain, thus preventing the propagation and growth of cracks in hydrogels (16).

However, simply mimicking the fibrous structure cannot replicate the combination of tissues' mechanical properties. For example, methods, such as microfluidics (17), wet spinning (18), and electrospinning (19), can produce micro-/nanofibers, but the formed fiber hydrogels or fiber mats are either too stiff such as electrospun polycaprolactone (PCL) fiber mats, or weak and brittle such as electrospun gelatin fibers (20). Introducing strong chemical crosslinks in and between the weak fibers enhanced their strength and toughness under a single cycle of mechanical load (21), but they were still susceptible to fatigue failures under multiple cycles of mechanical loads. The high fatigue resistance has been realized in tightly welded electrospun polyvinyl alcohol (PVA) nanofiber hydrogels via their high-density nanocrystalline domains (22), but the formed hydrogels had a low water content and a large Young's modulus.

This shows the importance of the molecular and nanostructure of microfibers. For example, by constructing a hierarchically anisotropy in fibrous structure, PVA hydrogels

Author affiliations: [a]Meinig School of Biomedical Engineering, Cornell University, Ithaca, NY 14853

Author contributions: M.W. designed research; M.W., S.S., G.D., and F.L. performed research; M.W. analyzed data; and M.W. and J.T.B. wrote the paper.

The authors declare no competing interest.

This article is a PNAS Direct Submission. C.S.C. is a guest editor invited by the Editorial Board.

[1]To whom correspondence may be addressed. Email: mw786@cornell.edu or jtb47@cornell.edu.

This article contains supporting information online at https://www.pnas.org/lookup/suppl/doi:10.1073/pnas.2213030120/-/DCSupplemental.

Published February 15, 2023.

achieved superior strength, toughness, and fatigue resistance (23). However, they showed inverse J-shaped stress–strain behaviors. By lowering the crystal content, mechanically aligned multiscale nanofibrous PVA hydrogels replicated the tissue-like J-shaped behaviors (24). However, this strategy is limited to the crystal-forming PVA. Such synthetic polymers do not have bioactivity to support and maintain cells living inside hydrogels, which are desired for next-generation biomaterials that contact cells and tissues (25, 26).

Gelatin-based hydrogels, especially gelatin methacryloyl (GelMA) hydrogels, have gained a widespread popularity for various biomedical applications (27, 28). They closely resemble some essential properties of native extracellular matrix (ECM) due to the presence of cell attaching and matrix metalloproteinase responsive peptide motifs. Here, we present a strategy to achieve the combinational soft tissue-like mechanical properties in GelMA via hierarchically designed GelMA microfibers. The gelatin fibers were fabricated by shear thinning of highly concentrated gelatin solution in highly viscous polymer flows. These fibers were functionalized and photocrosslinked into hydrogels. We tested the bioactivity of these hydrogels by seeding and culturing human adipose-derived stem cells (hASCs) and examining cellular mechanoresponses to different fiber architectures and mechanics.

Results

Fabrication of GelMA Fibers. To fabricate the metastable GelMA fibers, we prepared a PCL hollow tube with an inner diameter of D_0 and length of L_0 (*SI Appendix*, Fig. S1*A*) and highly concentrated gelatin solutions (40 to 50 wt%). We injected the gelatin into the tube and sealed two ends of the tubes. The gelatin-loaded PCL tube was heated to the melting temperature of PCL, 65 °C. The melting PCL is highly viscous and plastic, which allows large plastic deformations. We stretched the melting PCL tube to a total length of L (Fig. 1*A* and *SI Appendix*, Fig. S1*B*). After stretching, the PCL tube solidified when cooling to room temperature, and the gelatin inside the PCL tube was the as-formed fibers. The fibers were retrieved by dissolving PCL in acetone. They were then functionalized by methacrylic anhydride (MAA) in methanol to induce photocrosslinkable groups (Fig. 1*B*). To maximize the degree of functionalization, the weight ratio of MAA to gelatin fibers was above 2:1. In the meantime, concentration of MAA in methanol was kept below 1% and reaction time was less than 3 h to avoid MAA aggregation between fibers. The fiber diameter $D = D_0 \cdot \sqrt{L/L_0}$, is tunable. To mimic the microarchitecture of native tissues, we produced fibers with diameters from 1 μm (Fig. 1*C*) to 30 μm (Fig. 1*D*). To form hydrogels, the fibers were first hydrated in water containing photoinitiators, then molded and photocrosslinked into scaffolds by blue light.

During the thermomechanical process, the plastic deformation of melting PCL gradually aligned gelatin chains. Such alignment is metastable, and the chains will coil to random structures in water. However, acetone dehydrated the gelatin fibers when dissolving the PCL. Therefore, the metastable alignment of gelatin chains remained throughout the thermomechanical process and chemical functionalization. Upon hydration, the chains relax into high-entropy coil structures. Upon stretch, the high-entropy structure transformed to an aligned high-energy structure because the covalent crosslinks were built up when chains were aligned.

This GelMA fiber hydrogel (FiberGelMA) has a hierarchical structure: Sparsely bonded microfibers, whose polymer chains are crosslinked into metastable high-entropy random coils. The hierarchical structure has a great impact on the mechanical properties of FiberGelMA. The fiber diameter influences the equilibrium of gelatin chains: Chains are likely to be stabilized in thick fibers and unstable to form integrated bundles if the fibers are too thin. The welding density between fibers determines the stretchability of hydrogels, and whether individual fibers can fully extend to strengthen and toughen.

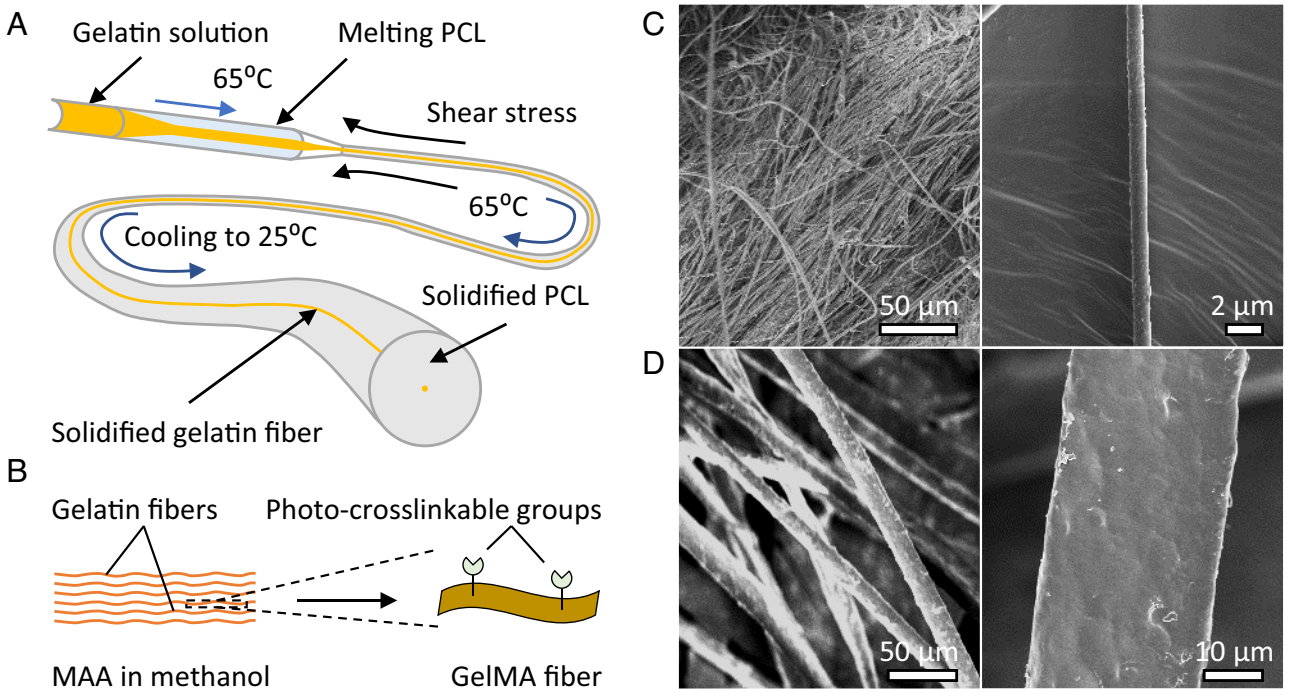

Fig. 1. Fabrication of GelMA fibers. (*A*) Gelatin solution was injected into a PCL tube and sealed in the tube. The tube melted at 65 °C and was drawn to elongate, before cooled to solidify. The gelatin solution was sheared to thinner and solidified to become fibers. (*B*) The fibers were functionalized by MAA in methanol to turn into GelMA fibers. (*C*) SEM images of GelMA fibers with diameters around 1 to 2 μm. (*D*) Fibers with diameters around 20 to 50 μm.

FiberGelMA Shows Soft Tissue-Like Combinational Mechanical Properties. We first studied the microarchitecture–mechanics relationship in FiberGelMA. The microfiber architecture fundamentally improved the ultimate tensile strength (UTS) and stretchability of GelMA. The FiberGelMA with 75 wt% water content reached a UTS of 1.1 ± 0.2 MPa and had a strain at break that was around 155 ± 41% (Fig. 2*A*). This is a striking contrast to traditional GelMA hydrogels (with the same water content as FiberGelMA), which had a UTS less than 0.05 MPa and could not sustain stretches with strains of over 50%. We also found that FiberGelMA prepared from fibers with a diameter of 20 μm was almost twice as strong as those with a diameter of 1 μm (Fig. 2*A*), showing that fiber architecture influences hydrogel mechanical properties. Another important feature of FiberGelMA's hierarchical structure is the crosslinks and welding between fibers. We adjusted the chances that fibers contacted and were crosslinked with each other by hydration ratios. FiberGelMA with water content of 50 wt% had much higher chance of intercrosslinked fibers, its UTS approached 2 MPa, but its stretchability was compromised, with a strain at break of below 75% (Fig. 2*B*). FiberGelMA with water content of 90 wt% was another extreme; although it was very stretchable, it was also weakest (Fig. 2*B*).

We then used FiberGelMA with fiber diameter of 20 μm and water content of 75 wt% for further tests on its fracture and fatigue resistance. The fracture energy of FiberGelMA was evaluated by pure shear tests (*SI Appendix*, Fig. S2), which have been widely used to test the resistance of rubbers and hydrogels to crack propagation (29, 30). Fracture of FiberGelMA was independent of the precut cracks (Fig. 2*D*), as polymer chains in fibers were completely insulated. This gives FiberGelMA a fracture energy of 9.2 ± 2.4 KJ/m^3, equaling its toughness per unit length.

The fatigue resistance of FiberGelMA was evaluated from two aspects. First, the resistance to creep fatigue was tested. Hydrogels were loaded in creep fatigue to 40% of UTS. They did not show the creep behaviors (Fig. 2*C*), maintaining the same peak cyclic strains with additional cycles. The resistance to crack growth was

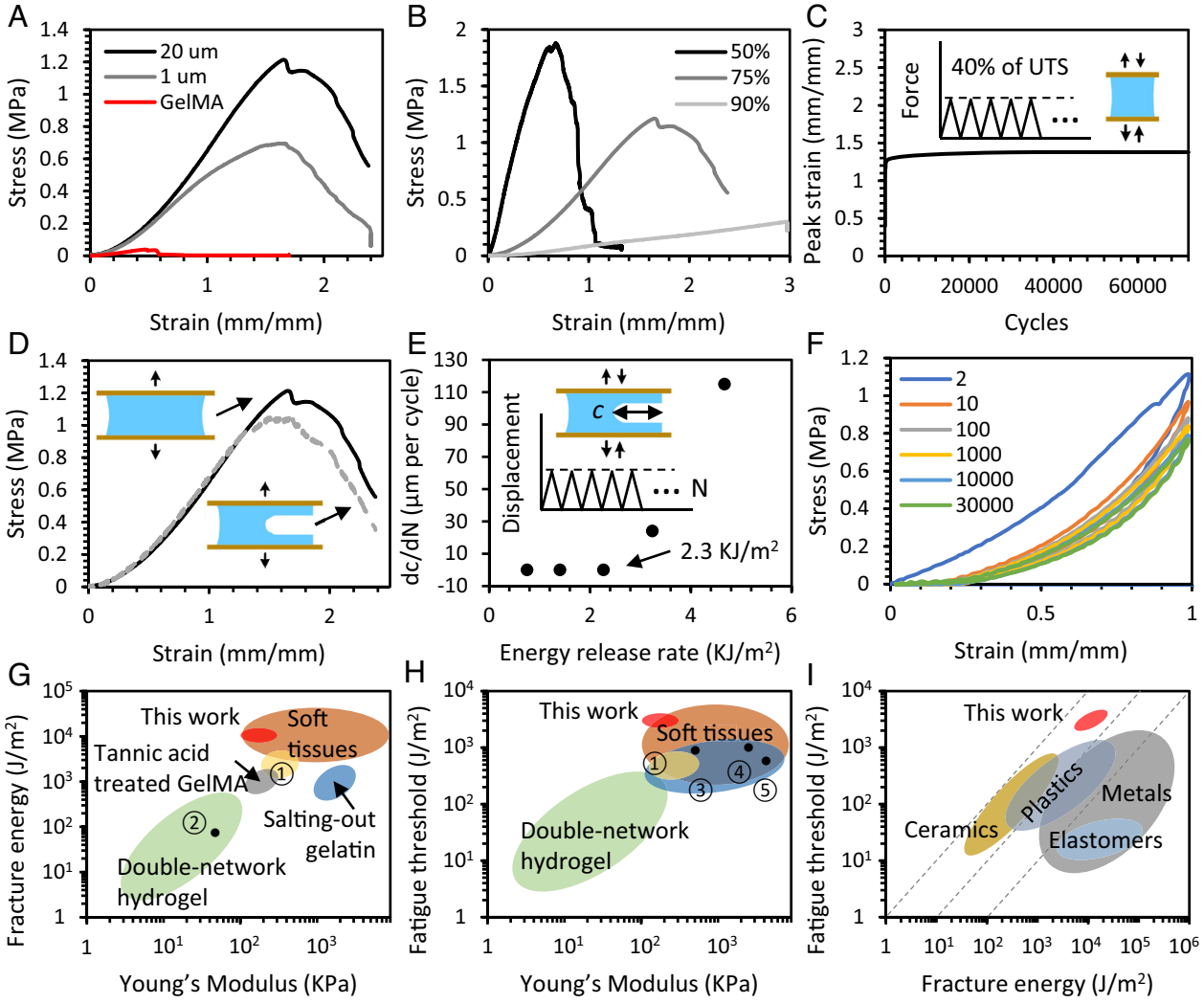

Fig. 2. Mechanical properties of GelMA fiber hydrogels. (*A*) Stress–strain curves of FiberGelMA prepared from GelMA fibers with diameters of 20 μm and 1 μm. The stress–strain curve of bulk GelMA hydrogels prepared by conventional methods is also shown here in red. (*B*) Stress–strain curves of FiberGelMA with different water content, which determined whether fibers were densely or sparsely intercrosslinked. (*C*) FiberGelMA was loaded in creep-fatigue to 40% of its ultimate tensile stress at 1 Hz for 72,000 cycles; it did not exhibit the creep behavior. (*D*) Stress–strain curves of FiberGelMA and notched FiberGelMA under uniaxial stretch. (*E*) The fatigue threshold was measured by pure shear tests, it is the maximum energy release rate without crack growth (dc/dN = 0). (*F*) Stress–strain curves of the FiberGelMA under cyclic loading to a strain of 100%. (*G*) Fracture energy – Young's Modulus, (*H*) Fatigue threshold—Young's Modulus, and (*I*) Fracture energy—Fatigue threshold charts compared FiberGelMA with reported high-performance hydrogels and various classes of materials. 1 PDMS fiber—PAAm hydrogel composite, 2 GelMA—Metro double-network, 3 Mechanically trained PVA, 4 Annealed PVA, 5 PVA nanofiber hydrogel.

also estimated by pure shear tests. Samples were loaded in cyclic fatigue to record the crack growth during each loading cycle dc/dN (*SI Appendix*, Fig. S3). The fatigue threshold is the maximum energy release rate G for dc/dN = 0, which is 2.3 ± 0.5 KJ/m^2 (Fig. 2*E*). Like native ECM, FiberGelMA exhibited nonlinear mechanical properties under cyclic loading (Fig. 2*F*), due to the rearrangement of micrometer-size fibers. It also exhibited a robust resilience, as the loading and unloading curves were close (Fig. 2*F*).

We compared FiberGelMA with two typical load-bearing soft tissues: skeletal muscles and ascending aortas (*SI Appendix*, Table S1). The FiberGelMA is soft as soft tissues but has a higher toughness and a fatigue threshold double of that of muscles and aortas.

We also compared FiberGelMA with other methods that enhance gelatin or GelMA, such as salting-out (11), which improves the toughness of gelatin by amplifying hydrophobic interactions and chain bundling, tannic acid treatment (31), which improves the toughness and stretchability of GelMA by inducing abundant hydrogen bonds, and double-network hydrogels formed between GelMA and methacrylated gellan gum (32), GelMA and methacrylated tropoelastin (33). FiberGelMA achieves a fracture energy that is two orders of magnitude larger than that of those enhanced gelatin or GelMA hydrogels, while being softer than most of them (Fig. 2*G*). Fatigue resistance has not yet been studied on those hydrogels, as their enhanced properties vanished under physiological conditions. For example, the salting-out gelatin swells in water and dissolves in 37 °C water. We instead compared the fatigue threshold of FiberGelMA with that of reported antifatigue hydrogels, including polydimethylsiloxane (PDMS) fiber-reinforced polyacrylamide (PAAm) hydrogel (29), annealed PVA (13), mechanically trained PVA (24), and PVA nanofiber hydrogels (22). FiberGelMA has the smallest Young's Modulus, but its fatigue threshold is more than double of that of most reported antifatigue hydrogels (Fig. 2*H*). When located among various classes of materials, FiberGelMA has the high fatigue threshold and fracture energy at the same order of magnitude (Fig. 2*I*), which are rarely found in traditional structural materials. More importantly, FiberGelMA can support and maintain live cells inside hydrogels, applicable to the emerging biomedical applications that PAAm and PVA hydrogels cannot fit.

Cells Spread in FiberGelMA and Form Interconnected 3D Meshwork. To evaluate the bioactivity of FiberGelMA, we seeded hASC in FiberGelMA. The dialyzed and lyophilized fibers are highly absorbent due to their porosity. They can absorb media up to 10 times their weight (Fig. 3*A*), to form a cell–fiber mixture. When the medium contains cells, this capillary action enables a uniform and 3D cell distribution in the mixture. The mixture was then molded and exposed to the light irradiation, which created covalent bonds in and between the hydrated fibers with the presence of the photoinitiator. The crosslinked hydrogel maintained the uniform cell distribution, as shown in the orthogonal projections of nuclei in confocal stacks across 100 μm depth (Fig. 3*B*). Cell density in each stack (850 μm × 850 μm) was counted, which remained around 1 million/cm^2 in most stacks

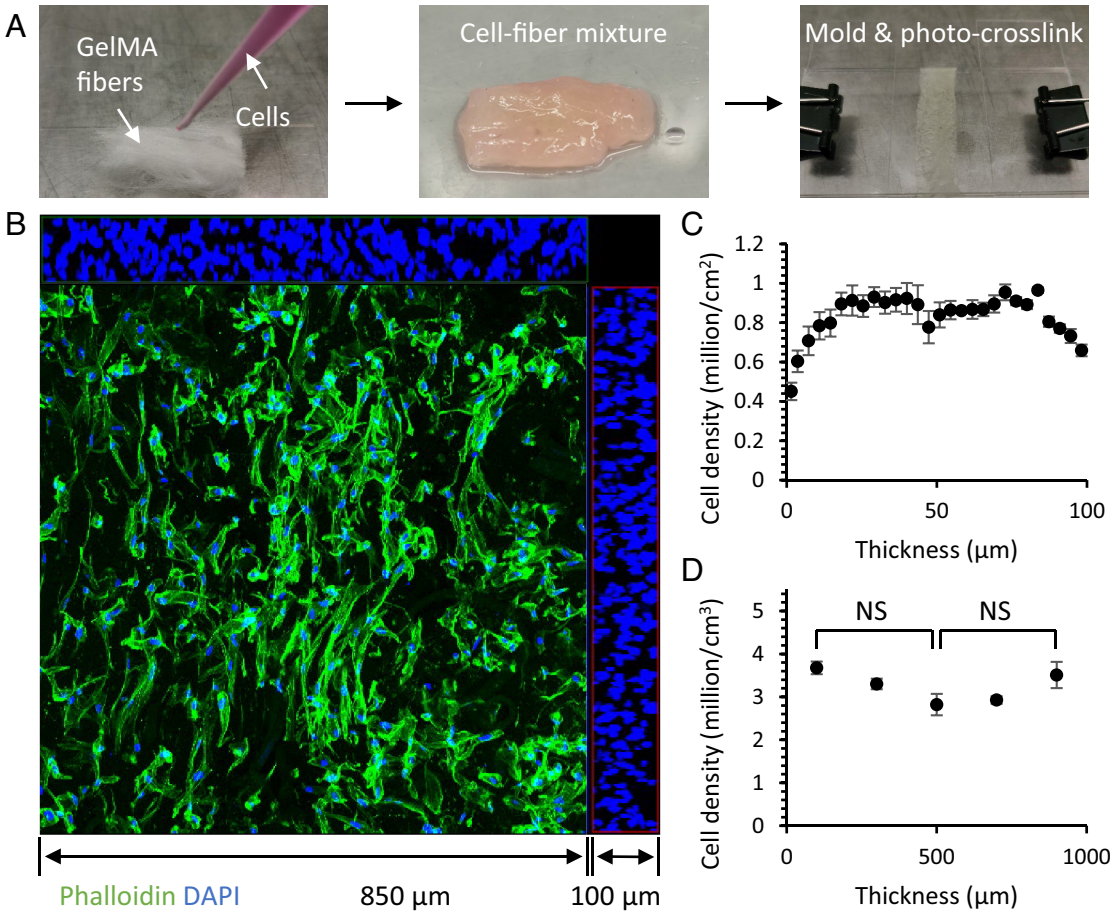

Fig. 3. Cells formed a uniform 3D meshwork in FiberGelMA. (*A*) For cell encapsulation, GelMA fibers were first hydrated with medium containing cells to form cell–fiber mixtures, which were then molded and photocrosslinked. (*B*) The 3D rendering of confocal stacks crosses a thickness of 100 μm, and the orthogonal projections of nuclei. (*C*) Cell density in each 2D stack throughout the 100 μm thickness. (*D*) Cell density in each 3D volume at different depths of a sample with a thickness of 1 mm. n = cells in a volume of 3 × 850 μm × 850 μm × 100 μm, significance is determined by Student *t* tests.

(Fig. 3*C*). This demonstrates that the FiberGelMA automatically supports microscopic cellularization. We further examined the macroscopic cell distribution across samples with a thickness of 1 mm. The samples were sectioned into sections with a thickness of 100 μm for confocal imaging. The 3D stacks (850 μm × 850 μm × 100 μm) taken at the different depths throughout 1 mm showed that the cell density was around 3 to 4 million/cm^3 (Fig. 3*D*), close to the seeding density of roughly 5 million/cm^3. This verified that FiberGelMA can provide uniform cell distribution across multiple scales. In the FiberGelMA, cells spread and built up an interconnected 3D meshwork in the FiberGelMA within as soon as 6 h (Fig. 3*B*). Such rapid formation of spreading cell meshwork has not been reported in conventional GelMA hydrogels, as it takes weeks for cells to degrade their surrounding gels before spreading.

FiberGelMA Architecture and Mechanics Direct Cellular Responses via Mechanically Gated Piezo1. We stretched the hASC-laden FiberGelMA in cyclic at 0.5 Hz for 48 h and compared the cellular responses to dynamic and static culture. Because of the shielding effect from microfibers, cell survival rate was not significantly impacted until the cyclic strain was over 50% (*SI Appendix*, Fig. S3).

Statically cultured hASCs were more contractile, as they had a higher expression of cytoskeletal F-actin (Fig. 4 *A*–*C*). Whereas, dynamically cultured cells were more stretched, as their length increased with cyclic strains (Fig. 4*E*). This led to different mechanosensing mechanisms. For cells cultured statically, YAP activation was significantly higher (Fig. 4*D*), and we have previously shown that the fiber diameter and alignment can regulate stem cell differentiation via YAP-mediated mechanotransduction (34). However, for cells cultured dynamically, their YAP was deactivated (Fig. 4*B*). Instead, the Piezo1 expression density increased with cyclic strains in a diameter-dependent manner (Fig. 4*F*).

To identify the role of Piezo1 in fiber mechanosensing, we performed gain-and-loss-of-function tests. For the gain-of-function tests, we encapsulated hASCs in FiberGelMA with fiber diameter of 20 μm and cultured samples under static conditions. Piezo1 agonist Yoda1 was added to the culture media at concentrations of

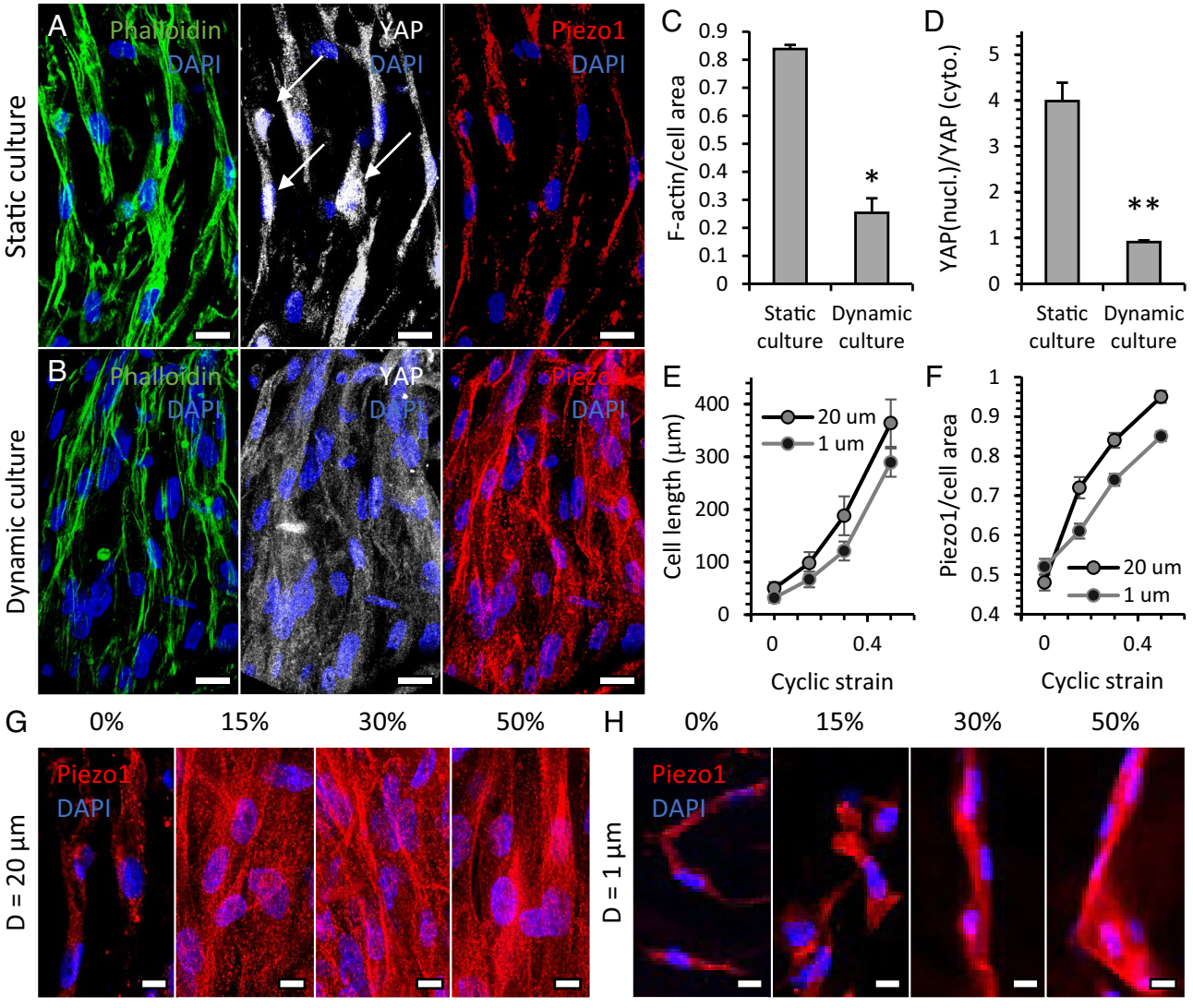

Fig. 4. Fiber architecture and mechanics-directed cellular mechanoresponses. (*A* and *B*) Immunofluorescence staining for YAP, Piezo1, and F-actin in cells cultured in FiberGelMA, (*A*) Samples were not loaded, (*B*) Samples were cyclic loaded to 50% strain. (*C*) Comparison between ratios of F-actin area to cell area, and (*D*) ratios of YAP densities inside to outside nuclei. (*E*) Cells were stretched by the cyclic loading, and their average length increased with peak strain. (*F*) Normalized Piezo1 intensity density also increased with cyclic strain. (*G* and *H*) Piezo1 expression in cells cultured in FiberGelMA with diameters of (*G*) 20 μm and (*H*) 1 μm, and loaded to strains of 0% (static culture), 15%, 30%, 50%. (*H*) (Scale bars, 20 μm.) n = cells in a volume of 3 × 212 μm × 212 μm × 50 μm, *P < 0.05, **P < 0.01, Student t tests.

0.2 μM, 2 μM, and 10 μM (*SI Appendix*, Fig. S5*A*). The Yoda1 elevated Piezo1 expression density (*SI Appendix*, Fig. S5*B*) and remarkably promoted cell elongation (*SI Appendix*, Fig. S5*C*). This "stretching" effect of Piezo1 activation was similar to the effect of cyclic loading on Piezo1 expression (Fig. 4*E*), and cell length (Fig. 4*F*). For the loss-of-function tests, we cultured cells transfected with Piezo1 small interfering RNA under dynamic conditions (*SI Appendix*, Fig. S5*D*). Both Piezo1 expression density (*SI Appendix*, Fig. S5*E*) and average cell length (*SI Appendix*, Fig. S5*F*) decreased significantly compared to nontransfected cells (Fig. 4 *E* and *F*).

Cells adjust their morphology in response to physical stimuli. The relations between Piezo1 activation/inhibition and cell elongation showed that Piezo1 plays a critical role in cellular response to cyclic stretch. Notably, the effects of cyclic stretch were valid only when fiber diameters were around the physiological range. When cells were cultured on fibers thicker than 200 μm or in fibers thinner than 200 nm, their Piezo1 expression and length were not significantly influenced by the cyclic loading (*SI Appendix*, Fig. S5 *G* and *H*). The Piezo1-mediated mechanotransduction has been shown to regulate the fate decision of neural and muscle stem cells (35, 36), and regulation of Piezo1 by fiber diameter and loading strain demonstrated the excellent bioactivity of FiberGelMA.

Discussion

Load-bearing soft tissues are soft, but are also strong, tough, and durable, owing to their hierarchical structures. In this paper, we present a strategy to resemble such structures and replicate the combination of mechanical and biological properties of load-bearing soft tissues in protein-based hydrogels. We created a hierarchical structure by mechanically shearing and crosslinking polymer chains into metastable microfibers. The metastable chains form high-entropy structures upon swollen and reversibly transform to stabilized high-energy structures upon stretch. The transition enables fibers to strengthen and toughen in a way similar to soft tissues. Unlike the widely adopted strategies that rely on the intra- and inter-polymer interactions provided by synthetic polymers (16), our method makes use of the long polymer chains itself. Since naturally derived hydrogels generally have long polymer chains, we speculate that this strategy may be widely applied to many other naturally derived hydrogels.

The hierarchical structure comprises microfibers which are sparsely bonded to allow individual fibers to extend to strengthen and toughen upon stretch. The strengthening and toughening originate from the nano- and molecular structures of fibers. Their metastable high-entropy structure (random coils) can reversibly transform to stabilized high-energy structures (helices). This transition enables fibers to be initially soft when the high-entropy structure bears the loads but ultimately strong as the high-energy structure takes the loads. This gives formed hydrogels a J-shaped stress–strain curve. The coil-helix transition also increased the stretchability of fibers and hence their toughness. The transition is reversible with no energy dissipation, preserving the structural integration of fibers under repeated cycles of loads. The synergy between microfibers and their metastable high-entropy polymer chains results in the combinations of soft tissue-like mechanical properties.

The fibrous architecture can locally interact with embedded cells and enhance their collaborative remodeling. For example, the fiber diameter and alignment regulate stem cell differentiation via focal adhesion-based mechanotransduction (34, 37). Here, we found that cells can also sense the stressed fibers but via mechanically gated ion channels. We propose a hypothesis for the divergent mechanisms in sensing static vs. stressed fibers. Cells are contractile when fibers relaxed (under minimal stress), and probe their elasticity by exerting contractile forces via focal adhesions and interpreting mechanical resistance (38, 39), this activates mechanoresponsive signaling pathways that stimulates nuclear translocation of transcription regulators such as YAP/Tafazzin (TAZ) (40, 41), and ultimately regulating cellular behaviors (42). However, cells are stretched when fibers are under cyclic stretch. This stress overwhelms the contractile forces cells can exert, and focal adhesions receive no feedback. On the contrary, the cell membrane is under stretch and could transmit stress to the mechanically gated ion channels on it (43, 44). Another hypothesis is that the consequence of prolonged cyclic stretch blunts transcriptional activity because of the inability of interacting proteins to "dock" dynamically (45).

Piezo1 is one of the major sensors of tissue stretch and regulates stem cell differentiation (46). However, an in-vitro study of Piezo1 in cellular responses to tissue stretch has been limited by available material systems that can resemble tissue mechanics and microarchitectures. FiberGelMA has great potential to fill this gap. Our results suggest that Piezo1 expression correlates to the nonlinear elasticity of stressed fibers, as it increases with broadening spectra of nonlinear elasticity. Since the nonlinear elasticity is a characteristic property of load-bearing soft tissues, this study may motivate future research on how tissue stretch regulates cellular responses via mechanically gated ion channels.

Many emerging biomedical applications, such as tissue engineering and cell-based therapies, rely heavily on cell seeding and culture. The FiberGelMA is cell friendly and enables uniform 3D cellularization inside hydrogels, and its high porosity also supports nutrition supplement for long-term culture. The rapid formation of interconnected 3D meshwork of cells is critical in applications that require mechanical or electrical connections between cells, such as regeneration of skeletal and cardiac muscles (47). With the tissue-like mechanical properties and rapid 3D cellularization, the cell-laden FiberGelMA could be implanted soon after cell seeding. This saves the long culture time and, more importantly, minimizes the maladaptive phenotype change due to long-term in-vitro culture. For example, chondrocytes started to show fibro-chondrocyte-like phenotype after weeks of in-vitro expansion and formed fibrocartilage instead of articular cartilage (48). Quiescent fibroblasts started to show myofibroblast-like contractile phenotype after long-term in-vitro culture and may lead to fibrotic and calcified tissues (49). The ECM-mimicking hierarchical structure could help cells retain their phenotype in addition to accelerating the culture time to achieve material properties.

In conclusion, we present a strategy for making the soft, strong, tough, and durable hydrogels from naturally derived materials. We demonstrate the importance of creating hierarchical structure with minimal crosslinks that can avoid stress localization. By this strategy, we create the FiberGelMA with a combination of tissue-like mechanical, biological, and architectural properties. It supports rapid formation of 3D cell meshwork and regulates cellular responses by fiber architecture and mechanics. Combination of these properties is highly desirable for various biomedical applications such as wound healing and soft-tissue engineering. This work sets a paradigm for the next-generation biomaterials.

Materials and Methods

Fiber Fabrication and Hydrogel Preparation. Gelatin (Sigma) solution (20 to 40 wt%) was injected into a PCL tube, which was made from moldable plastic pellets (Amazon). The tube was then sealed and heated to 65 °C to melt both PCL and gelatin. The melting tube was repeatedly stretched and folded to thinning the inner gelatin solution to target diameter. When cooling at room temperature, the PCL tube solidified, and the gelatin solution became strands of gel fibers. The fibers were retrieved by dissolving the PCL in acetone. They were methacrylated by 1 v/v%

MAA in methanol for 1 h. The functionalized fibers were dialyzed in DI water through a 12 to 14 KDa membrane for 5 d and lyophilized for 3 d. To form hydrogels, the dry and sterile fibers were hydrated in water or medium at a weight ratio of 1:3 to 1:8. The water contains 0.05 to 0.5 wt% photoinitiator LAP (lithium phenyl-2,4,6-trimethylbenzoylphosphinate). The fibers became hydrophilic after the MAA treatment and absorbed water by capillary action. The water-absorbent fibers were molded and photocrosslinked upon light irradiation (365 to 400 nm, 2.5 mW/cm^2, 5 min).

Mechanical Tests of Hydrogels. A Mark-10 F105 with a 250-N load sensor was used for mechanical tests. The uniaxial tensile tests were used to measure the ultimate tensile stress, Young's modulus, and toughness. Samples (width: 10 mm, length between two grippers: 20 mm, thickness: around 1 mm) were loaded at a strain rate of 2% /s until fracture. The ultimate tensile stress is the maximum stress samples can sustain. Young's modulus is the slope of stress–strain curves. The toughness is the area under stress–strain curves before fracture. The pure shear tests were used to measure the fracture energy (*SI Appendix*, Fig. S2*A*) and fatigue threshold (*SI Appendix*, Fig. S3*A*). For fracture energy measurement, each group had two identical samples (width: 50 mm, length between two grippers: 10 mm, thickness: around 1 mm). They were loaded in uniaxial tension at a strain rate of 2% /s until fracture. The notched sample with a 15-mm precut crack was used to find the critical strain, while the unnotched sample was used to measure the stress–strain curve (*SI Appendix*, Fig. S2*B*). The fracture energy = the area under stress–strain curves before the critical strain × 10 mm. For fatigue threshold measurement, samples in each group were loaded in cyclic fatigue to the same strain at a frequency of 1 Hz for 30,000 cycles. The notched sample was used to record the crack growth by each loading cycle d*c*/d*N*, while the unnotched sample was used to measure the stress–strain curve (*SI Appendix*, Fig. S3*B*). The energy release rate G = the area under stress–strain curves × 10 mm. The fatigue threshold is the maximum G for d*c*/d*N* = 0 (*SI Appendix*, Fig. S3*C*). The creep-fatigue tests were used to evaluate the creep behavior. Samples (width: 10 mm, length between two grippers: 20 mm, thickness: around 1 mm) were loaded in creep-fatigue to 40% of their ultimate tensile stress at a frequency of 1 Hz. The peak strain of each cycle was plotted and determined whether samples showed the creep behavior.

Scanning Electron Microscopy. Zeiss Gemini 500 was used to show the morphology of dry fibers. The samples were first coated with gold-platinum, and then imaged under the electron beam intensity at 2 kV.

Cell Culture. hASCs were purchased from Lonza and Passage-5 cells were used. The cells were first suspended in the culture medium containing 0.05% LAP, and then dropped onto fibers at a seeding density of 5 million/cm^3. Fibers absorbed the medium and cells by capillary action. The mixture was first incubated for 30 min and then molded and photocrosslinked. The samples were cultured in the culture medium for 24 h before dynamic or static culture for 48 h. For dynamic culture, the hydrogels were cyclic stretched to nominal strains of 15%, 30%, and 50%. The culture medium was prepared by supplementing Dulbecco's modified Eagle medium (Invitrogen) with 10% fetal bovine serum (FBS, Invitrogen) and 1% penicillin/streptomycin (P/S, Invitrogen).

Immunofluorescence Staining. Samples were fixed in 4% paraformaldehyde in PBS for 15 min at room temperature and permeabilized with 0.05% Triton X-100 in PBS for 15 min. They were then blocked with 1% BSA in PBST for 1 h, before incubated with primary antibodies against Yes Associated Protein (YAP) (1:200, mouse, Santa Cruz sc-101199) and Piezo1 (1:200, Rabbit, Proteintech 15939-1-AP), or α-SMA (1:200, rabbit, Invitrogen) and Vimentin (1:200, mouse, Sigma) overnight at 4 °C. After rinse, the samples were incubated with secondary antibodies (1:200; AlexaFluor-555/647; Invitrogen) at room temperature for 1 h. The cytoskeleton was stained by AlexaFluor 488 conjugated phalloidin (Invitrogen), and cell nuclei were labeled by 4′,6-diamidino-2-phenylindole (DAPI) (Invitrogen). Confocal images were taken by Zeiss LSM 710.

Image Analysis and Statistics. ImageJ was used for image analysis. Nuclei were counted in each stack of confocal images for estimation of the 2D cell density. The 3D object algorithm was used to count nuclei in 3D stacks. YAP/TAZ localization was estimated by the ratio between the densities of YAP signals inside and outside nuclei. A ratio much higher than one represents YAP activation, while a ratio smaller than one indicates that YAP is deactivated. Piezo1 intensity density was estimated by dividing the average intensity of Piezo1 by cell areas. The higher the density is, the more Piezo1 is activated. For significance analysis between two groups, the two-tailed Student *t* test was used.

Data, Materials, and Software Availability. All study data are included in the article and/or *SI Appendix*.

ACKNOWLEDGMENTS. This work was supported by American Heart Association (grant 821615 to M.W.), NIH (grants HL128745, HL143247, and HL160028 to J.T.B.), Biotechnology Resource Center Imaging Facility (RRID:SCR_ 021741) of the Cornell Institute of Biotechnology, and Cornell Center for Materials Research Shared Facilities which are supported through the NSF Materials Research Science and Engineering Center (MRSEC) program (DMR-1719875).

1. M. Vatankhah-Varnosfaderani *et al.*, Mimicking biological stress–strain behaviour with synthetic elastomers. *Nature* **549**, 497–501 (2017).
2. A. J. Bailey *et al.*, Viscoelastic properties of collagen: Synchrotron radiation investigations and structural model. *Philos. Trans. R. Soc. Lond. B Biol. Sci.* **357**, 191–197 (2002).
3. A. J. Bailey *et al.*, Elastic proteins: Biological roles and mechanical properties. *Philos. Trans. R. Soc. Lond. B Biol. Sci.* **357**, 121–132 (2002).
4. M. A. Lillie, J. M. Gosline, Limits to the durability of arterial elastic tissue. *Biomaterials* **28**, 2021–2031 (2007).
5. M. J. Harrington, P. Fratzl, Natural load-bearing protein materials. *Progr. Mater. Sci.* **120**, 100767 (2021).
6. W. Kong *et al.*, Muscle-inspired highly anisotropic, strong, ion-conductive hydrogels. *Adv. Mater.* **30**, 1801934 (2018).
7. M. Jaspers *et al.*, Ultra-responsive soft matter from strain-stiffening hydrogels. *Nat. Commun.* **5**, 5808 (2014).
8. M. Vatankhah-Varnosfaderani *et al.*, Chameleon-like elastomers with molecularly encoded strain-adaptive stiffening and coloration. *Science* **359**, 1509–1513 (2018).
9. X. Hu, M. Vatankhah-Varnoosfaderani, J. Zhou, Q. Li, S. S. Sheiko, Weak hydrogen bonding enables hard, strong, tough, and elastic hydrogels. *Adv. Mater.* **27**, 6899–6905 (2015).
10. J.-Y. Sun *et al.*, Highly stretchable and tough hydrogels. *Nature* **489**, 133–136 (2012).
11. Q. He, Y. Huang, S. Wang, Hofmeister effect-assisted one step fabrication of ductile and strong gelatin hydrogels. *Adv. Funct. Mater.* **28**, 1705069 (2018).
12. R. Bai, J. Yang, Z. Suo, Fatigue of hydrogels. *Euro. J. Mech.–A/Solids* **74**, 337–370 (2019).
13. S. Lin *et al.*, Anti-fatigue-fracture hydrogels. *Sci. Adv.* **5**, eaau8528 (2019).
14. U. G. K. Wegst, H. Bai, E. Saiz, A. P. Tomsia, R. O. Ritchie, Bioinspired structural materials. *Nat. Mater.* **14**, 23–36 (2015).
15. F. Burla, Y. Mulla, B. E. Vos, A. Aufderhorst-Roberts, G. H. Koenderink, From mechanical resilience to active material properties in biopolymer networks. *Nat. Rev. Phys.* **1**, 249–263 (2019).
16. X. Zhao *et al.*, Soft materials by design: Unconventional polymer networks give extreme properties. *Chem. Rev.* **121**, 4309–4372 (2021).
17. J. Cheng, Y. Jun, J. Qin, S.-H. Lee, Electrospinning versus microfluidic spinning of functional fibers for biomedical applications. *Biomaterials* **114**, 121–143 (2017).
18. B. Kong *et al.*, Tailoring micro/nano-fibers for biomedical applications. *Bioactive Mater.* **19**, 328–347 (2023).
19. J. Xue, T. Wu, Y. Dai, Y. Xia, Electrospinning and electrospun nanofibers: Methods, materials, and applications. *Chem. Rev.* **119**, 5298–5415 (2019).
20. R. J. Wade, E. J. Bassin, W. M. Gramlich, J. A. Burdick, Nanofibrous hydrogels with spatially patterned biochemical signals to control cell behavior. *Adv. Mater.* **27**, 1356–1362 (2015).
21. D. C. Schoenmakers, A. E. Rowan, P. H. J. Kouwer, Crosslinking of fibrous hydrogels. *Nat. Commun.* **9**, 2172 (2018).
22. J. Ni *et al.*, Strong fatigue-resistant nanofibrous hydrogels inspired by lobster underbelly. *Matter* **4**, 1919–1934 (2021).
23. M. Hua *et al.*, Strong tough hydrogels via the synergy of freeze-casting and salting out. *Nature* **590**, 594–599 (2021).
24. S. Lin, J. Liu, X. Liu, X. Zhao, Muscle-like fatigue-resistant hydrogels by mechanical training. *Proc. Natl. Acad. Sci. U.S.A.* **116**, 10244–10249 (2019).
25. X. Han *et al.*, Biomaterial-assisted biotherapy: A brief review of biomaterials used in drug delivery, vaccine development, gene therapy, and stem cell therapy. *Bioact. Mater.* **17**, 29–48 (2022).
26. A. L. Facklam, L. R. Volpatti, D. G. Anderson, Biomaterials for personalized cell therapy. *Adv. Mater.* **32**, 1902005 (2020).
27. A. G. Kurian, R. K. Singh, K. D. Patel, J.-H. Lee, H.-W. Kim, Multifunctional GelMA platforms with nanomaterials for advanced tissue therapeutics. *Bioact. Mater.* **8**, 267–295 (2022).
28. K. Yue *et al.*, Synthesis, properties, and biomedical applications of gelatin methacryloyl (GelMA) hydrogels. *Biomaterials* **73**, 254–271 (2015).
29. C. Xiang *et al.*, Stretchable and fatigue-resistant materials. *Mater. Today* **34**, 7–16 (2020).
30. Z. Wang *et al.*, Stretchable materials of high toughness and low hysteresis. *Proc. Natl. Acad. Sci. U.S.A.* **116**, 5967–5972 (2019).
31. B. Liu *et al.*, Hydrogen bonds autonomously powered gelatin methacrylate hydrogels with super-elasticity, self-heal and underwater self-adhesion for sutureless skin and stomach surgery and E-skin. *Biomaterials* **171**, 83–96 (2018).
32. H. Shin, B. D. Olsen, A. Khademhosseini, The mechanical properties and cytotoxicity of cell-laden double-network hydrogels based on photocrosslinkable gelatin and gellan gum biomacromolecules. *Biomaterials* **33**, 3143–3152 (2012).
33. N. Annabi *et al.*, Engineered cell-laden human protein-based elastomer. *Biomaterials* **34**, 5496–5505 (2013).
34. M. Wang *et al.*, Regulating mechanotransduction in three dimensions using sub-cellular scale, crosslinkable fibers of controlled diameter, stiffness, and alignment. *Adv. Funct. Mater.* **29**, 1808967 (2019).
35. N. Ma *et al.*, Piezo1 regulates the regenerative capacity of skeletal muscles via orchestration of stem cell morphological states. *Sci. Adv.* **8**, eabn0485 (2022).

36. M. M. Pathak *et al.*, Stretch-activated ion channel Piezo1 directs lineage choice in human neural stem cells. *Proc. Natl. Acad. Sci. U.S.A.* **111**, 16148–16153 (2014).
37. B. R. Seo *et al.*, Collagen microarchitecture mechanically controls myofibroblast differentiation. *Proc. Natl. Acad. Sci. U.S.A.* **117**, 11387–11398 (2020).
38. L. Li, J. Eyckmans, C. S. Chen, Designer biomaterials for mechanobiology. *Nat. Mater.* **16**, 1164–1168 (2017).
39. K. H. Vining, D. J. Mooney, Mechanical forces direct stem cell behaviour in development and regeneration. *Nat. Rev. Mol. Cell Biol.* **18**, 728–742 (2017).
40. G. Brusatin, T. Panciera, A. Gandin, A. Citron, S. Piccolo, Biomaterials and engineered microenvironments to control YAP/TAZ-dependent cell behaviour. *Nat. Mater.* **17**, 1063–1075 (2018).
41. S. Dupont *et al.*, Role of YAP/TAZ in mechanotransduction. *Nature* **474**, 179–183 (2011).
42. A. Totaro, T. Panciera, S. Piccolo, YAP/TAZ upstream signals and downstream responses. *Nat. Cell Biol.* **20**, 888–899 (2018).
43. H. De Belly, E. K. Paluch, K. J. Chalut, Interplay between mechanics and signalling in regulating cell fate. *Nat. Rev. Mol. Cell Biol.* **23**, 465–480 (2022).
44. J. M. Kefauver, A. B. Ward, A. Patapoutian, Discoveries in structure and physiology of mechanically activated ion channels. *Nature* **587**, 567–576 (2020).
45. R. A. Gould *et al.*, Cyclic mechanical loading is essential for Rac1-mediated elongation and remodeling of the embryonic mitral valve. *Curr. Biol.* **26**, 27–37 (2016).
46. L. He, G. Si, J. Huang, A. D. T. Samuel, N. Perrimon, Mechanical regulation of stem-cell differentiation by the stretch-activated Piezo channel. *Nature* **555**, 103–106 (2018).
47. K. Elkhoury *et al.*, Biofabrication of natural hydrogels for cardiac, neural, and bone tissue engineering applications. *Bioact. Mater.* **6**, 3904–3923 (2021).
48. H.-P. Lee, L. Gu, D. J. Mooney, M. E. Levenston, O. Chaudhuri, Mechanical confinement regulates cartilage matrix formation by chondrocytes. *Nat. Mater.* **16**, 1243–1251 (2017).
49. E. S. Fioretta *et al.*, Next-generation tissue-engineered heart valves with repair, remodelling and regeneration capacity. *Nat. Rev. Cardiol.* **18**, 92–116 (2021).